Available online at www.sciencedirect.com
SCIENCE DIRECT
Catalysis Today 105 (2005) 85–92
CATALYSIS TODAY
www.elsevier.com/locate/cattod

A density functional theory study of the adsorption of acetone to the (1 1 1) surface of Pt: Implications for hydrogenation catalysis

Edward L. Jeffery, Rajinder K. Mann, Graham J. Hutchings, Stuart H. Taylor, David J. Willock *

Department of Chemistry, Cardiff University, P.O. Box 912, Cardiff CF10 3TB, UK

Abstract

We present periodic density functional theory calculations on the adsorption modes of acetone over the (1 1 1) surface of Pt. The dominant species previously observed in low temperature HREELS and RAIRS experiments is an ''end-on'' η^1(O)-ketone and the calculated adsorption energy and vibrational frequencies for this species agree well with the literature data. The secondary species reported previously has been assigned to a η^2(C_2,O)-ketone with the molecular plane parallel to the surface. We show that this is an unlikely assignment and suggest an alternative enolate structure which has calculated vibrational frequencies in agreement with the spectra. The implications of the adsorption modes proposed in this work for models of the enantioselective hydrogenation of pyruvate esters are discussed.

Keywords: pDFT; Acetone; Hydrogenation catalysis; Enolate

1. Introduction

The adsorption of acetone to the surface of group 10 hydrogenation catalysts provides a basic model system to study the adsorption and reaction of ketone containing molecules. The insight provided by modelling in this area can provide a start point for determining the likely mechanism for difficult problems of stereo-selectivity and regio-selectivity in molecules containing more than one multiple bond. For example, the hydrogenation of methyl pyruvate is known to undergo enantioselective hydrogenation in the presence of cinchonidine and related modifiers. The most widely used picture of the selective step in these reactions involves a surface dimer formed between the keto-ester and the modifier which controls the direction from which hydrogen is delivered to one face of the ketone group [1]. These models depend on the dimer structure being determined by inter-molecular forces, the interaction with the metal surface is either ignored completely or included only as a geometric constraint. Recently, cluster DFT models have been presented which use optimisations of large subunits of modifier and substrates to take surface interactions into account [2] but modelling of the complete system has still not been successfully attempted.

The dimer model assumes that the ketone group to be hydrogenated is adsorbed parallel to the surface so that the direction of the delivery of H is easily predicted. However, thermal desorption spectra (TDS) and HREELS experiments of acetone on single crystals suggested that the dominant species on the (1 1 1) surface has a η^1(O) end-on adsorption geometry in which the oxygen atom is bonded to the surface with the C=O bond almost perpendicular to the surface [3]. A small quantity of a η^2(C,O) adsorbed species in which the carbonyl group is parallel to the surface is implied from the spectra, but the concentration is indicative of this being located at defect sites, such as step edges. This dominance of an end-on adsorption mode has also been confirmed by more recent RAIRS and HREELS experiments on almost defect free Pt(1 1 1) [4]. It is the aim of this work to use computer modelling to consider the adsorption mode of acetone on Pt(1 1 1), and to discuss the implications of this for models of hydrogenation selectivity.

Simulation of the adsorption process of acetone on Pt surfaces can be found in the literature. Semi-empirical Hückel theory calculations have been used to simulate the

* Corresponding author. Tel.: +44 2920 874 779; fax: +44 2920 874 030.
E-mail address: willockdj@cf.ac.uk (D.J. Willock).

0920-5861/$ – see front matter
doi:10.1016/j.cattod.2005.04.013

adsorption of acetone and propanone to Pt and Pd systems by Delbecq and Sautet [5]. They considered six adsorption modes, three for η^1(O) and three for η^2(C,O) which varied according to the co-ordination of the adsorbate with surface atoms. A preference for η^1(O) acetone to occupy a top site position, interacting with a single Pt atom, and for the η^2(C,O) adsorbate to take on a di-σ mode, with C and O atoms bonded to neighbouring Pt sites, was identified. More recently, Vargas et al. [2] have considered the adsorption of acetone to a 19 atom cluster model of Pt(1 1 1). Again they consider the η^1(O) and di-σ η^2(C,O) adsorption and find similar adsorption geometries to the earlier work. In the η^2(C,O) mode, the C=O bond is longer than in the gas-phase ketone and closer to the C–O bond length in a reference calculation on 2-propanol. Previous periodic density functional theory calculations have been based on a two-layer slab model with only the adsorbate atoms geometry optimised. These confirm that, for acetone, the η^2(C,O) parallel adsorption geometry is less energetically favourable than the η^1(O) end-on structure [6]. For formaldehyde, the reverse energetic ordering is found and so it is likely that the steric interaction of the methyl groups with the (1 1 1) surface is responsible for de-stabilising the η^2(C,O) structure for acetone. However, this steric interaction may be exaggerated by the use of a fixed surface.

Although the keto-isomer is usually assumed to be the important reactant form in pyruvate hydrogenation there are observations that more complex adsorption modes may be possible. In particular Wells and co-workers [7] have studied methyl pyruvate hydrogenation over modified Pd (4% Pd on Fe_2O_3) at 293 K and 10 bar pressure. The enantiomeric excesses observed were smaller and in the opposite sense to the corresponding reactions over Pt, i.e. on Pd cinchonine gave *R*-product in excess while cinchonidine gave *S*-product. In addition D-tracer experiments, in which the reaction was carried out in deuterated solvents and with D_2 in place of H_2 in the feed, showed deuteration on the methyl group of the pyruvate substrate that was not observed in the corresponding reactions over Pt. This implies that hydrogenation is taking place via the enol-isomer of the reactant on the Pd surface. Reaction of molecules containing both C=C and C=O functional groups, e.g. but-3-en-2-one also showed that the former bond was hydrogenated at a much faster rate than the ketone group over the Pd catalyst. So that on Pd, the enol form of the reactant can be formed under the reaction conditions and once this transformation has taken place the C=C group is hydrogenated rapidly. For the model system of acetone, there are also recent results from RAIRS experiments showing that an enolate species can be formed on the (1 1 1) surface of Ni [8].

In this paper, we will use periodic density functional theory to study the adsorption of acetone on the Pt(1 1 1) surface. A three-layer slab model is employed and full relaxation of metal and adsorbate atoms is employed throughout. We will consider the relative energetics of adsorption in ketone, enol and enolate-isomers using a common gas phase ketone reference state. Direct comparison of calculated vibrational modes will be made with the available HREELS and RAIRS data.

The adsorption geometries reported in the literature so far have used a system of nomenclature drawn from the concept of hapticity used in organometallic chemistry. We have already referenced structures of η^1(O) and η^2(C,O) types from earlier work. In this paper, we will also use of the symbol μ_n to indicate that the adsorbate is bridging *n* surface metal atoms. In this way, ambiguities can be removed such as the distinction between η^2(C,O) in which both C and O interact with a single metal atom (a π adsorbed mode) and μ_2(C,O) in which C and O interact with different metal centres (a di-σ adsorbed mode).

2. Computational details

The calculations presented here employ density functional theory with the generalised gradient approximation (GGA-DFT), as implemented in the code VASP [9] (Vienna Ab initio Simulation Program). The exchange and correlation energies are described using the parameterisation of Perdew et al., PW91 [10]. A plane wave basis set was used with three dimensional periodic boundary conditions applied to the simulation; a plane wave cut-off of 400 eV was found to be sufficient for all calculations. Core states of all atoms in the simulation were represented using projector augmented-wave (PAW) pseudo-potentials [11] which, in common with the earlier ultra-soft pseudopotentials used in the VASP code [12], have been parameterised with reference to all electron calculations that included scalar relativistic effects for heavy elements such as Pt [11,12]. Treatment of relativistic effects for the core electrons is important to correctly reproduce the well known core contraction for the heavy elements which has a significant impact on the interaction of adsorbates with the surfaces studied here and manifests itself in the catalysis of group 10 metals [13].

The fcc bulk unit cells of each metal were optimised using a $5 \times 5 \times 5$ *k*-points sampling grid in reciprocal space. The *k*-points were positioned and weighted using the Monkhurst-Pack [14] scheme with convergence of the total energy with respect to *k*-point sampling accelerated using second order Methfessel-Paxton smearing with a width of 0.1 eV. This produced a calculated equilibrium lattice constant of 3.986 Å, in good agreement with the experimental value of 3.924 Å.

For surface simulations the bulk cell was re-orientated so that the *c*-direction of the simulation cell was perpendicular to the (1 1 1) surface. A vacuum gap of 15 Å was then introduced to ensure that adsorbates do not interact with the periodic images of the metal slab. All surface calculations presented in the Results section are based on the full relaxation of a $p(3 \times 3)$ slab 3 atomic layers deep containing 27 metal atoms. The $p(3 \times 3)$ slab super-cell is hexagonal with dimensions $a = b = 8.4314$ Å, $c = 19.5895$ Å, includ-

ing the vacuum gap. Convergence of the adsorption energies required a *k*-point sampling of 3 × 3 × 1. This is consistent with the 5 × 5 × 5 *k*-point grid used for bulk convergence since the surface slab is a larger real space simulation cell. In addition only 1 *k*-point is required in the direction perpendicular to the slab surface.

Test calculations show that the size of simulation cell employed is a good compromise between accuracy and computational speed. For example, a calculation using a $p(4 \times 4)$, five-layer simulation, for the $\mu_2(C_2,O)$ acetone adsorption geometry, gave an adsorption energy within 4 kJ mol^{-1} of our standard method. This is consistent with our earlier calculations on the adsorption of hydrogen to Ni, Pd and Pt in which we also found only minor changes in the calculated adsorption energies for the computationally more expensive five-layer slab [15].

For relaxations of the slab model the cell vectors are fixed to prevent the collapse of the vacuum gap and to preserve the periodicity of the bulk termination. However, all metal atoms in the slab are relaxed. In effect this means that the lower surface atom co-ordinates can, in principle, respond to the presence of the adsorbate. In our experience, this effect is small; the adsorption energy of acetone in the $\mu_2(C_2,O)$ structure using a three-layer slab with the third-layer atoms fixed at their relaxed bulk co-ordinates differed from the value obtained with all atom positions optimised by less than 3 kJ mol^{-1}.

From these test calculations, we conclude that the $p(3 \times 3)$ three-layer slab provides a reliable system size for the considerable number of calculations undertaken in this work. In this regard, it was also interesting to note that for the relaxed clean (1 1 1) surface of Pt, the interlayer spacing was found to increase from 2.301 Å in the bulk to 2.323 Å, an increase of +0.94%, in excellent agreement with the experimentally observed change of +0.9% [16].

To calculate the adsorption energy of molecular species we use the formula:

$$E_{ads} = -(E_{MS} - E_M - E_S) \quad (1)$$

where E_{MS} is the total calculated energy for the adsorbate on the surface, E_S is the calculated energy for the surface without the adsorbate present and E_M is a reference calculation on the isolated molecule. For all three calculations, the same simulation cell dimensions, basis set cut off energies and *k*-point sampling are employed, set at the values determined for the clean surface as detailed above. For each calculation of the adsorbate on the surface and the reference states full optimisation of the atomic degrees of freedom is allowed but the simulation cell dimensions are set from the optimised bulk structure. In the case of acetone, several isomers are considered but the reference gas phase state is always taken as the keto-isomer which is found to be lower in energy than the enol form by 49 kJ mol^{-1}. This gives a common reference state for all surface adsorbates considered, so that the adsorption energy of the enol-isomer, for example, includes the energy required to convert a gas phase ketone into the enol form.

Table 1
Calculated energies and geometric parameters for gas phase species

	E_{rel}[a] (kJ mol^{-1})	C_2–O (Å)	C–C_2 (Å)	CC_2O (°)
Keto-isomer	0	1.23	1.51	121
Enol-isomer	49.2	1.38	1.34/1.50	125/111
Enolate-ion	254.7	1.28	1.39/1.54	126/116

[a] Energy relative to keto-isomer.

Vibrational modes of the adsorbed molecules were calculated using a numerical three point approach with atomic displacements of 0.04 Å, only the co-ordinates of the adsorbate atoms were included as degrees of freedom. The validity of using this reduced dynamical matrix was checked by extending an example calculation to include co-ordinated surface atoms, this lead to only negligible changes in the observed vibrational frequencies.

3. Results and discussion

To consider the full range of isomers of acetone that can be present on the metal surface we consider not only the keto-isomer (Fig. 1a) but also the enol-isomer (Fig. 1b) and the enolate form (Fig. 1c). The enolate is formally an anionic species generated by proton abstraction from the alcohol group of the enol-isomer. For simulation of adsorption modes of the enolate, we also included a hydrogen atom, placed as far from the enolate moiety as possible in the simulation cell employed. Reference calculations of the three forms in the gas phase are summarised in Table 1, which shows that the keto-isomer is the most stable form with the enol-isomer some 49 kJ mol^{-1} higher in energy. For the enolate-ion, the reference calculation used the anion in a unit cell with a uniform positive background charge to give an overall neutral repeat unit. For the gas phase, this provides a considerably more stable solution than the alternative with H included explicitly in the simulation cell. This is not surprising since the energy of abstraction of H in a reaction depends strongly on the species receiving the H atom. In the surface adsorption calculations, the fate of the abstracted H atom is adsorption to the metal surface but the correct treatment of H is less clear for this reference gas phase data and the uniform background charge is at least a well defined state. The abstraction represented in this way produces a structure with a calculated energy 255 kJ mol^{-1} higher than the ketone-isomer.

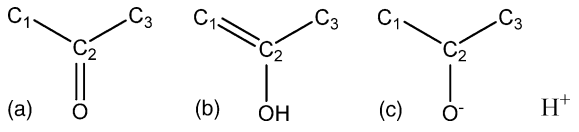

Fig. 1. The molecular species considered in this study for the adsorption of acetone. (a) Keto-isomer, (b) enol-isomer and (c) enolate-ion, H atoms on carbon have been omitted for clarity.

Table 2
Energies and geometric parameters from the optimised structures of acetone adsorption on Pt(1 1 1)

	E_{ads}[a] (kJ mol^{-1})	C_2–O (Å)	C_1–C_2 (Å)	M–O (Å)	M–C (Å)	CC_2O[b] (°)	CCC–O[c] (°)	C_2–X–M[d] (°)	Δz M[e] (Å)
Ketone $\mu_2(C_2,O)$	20.5	1.38	1.52	2.04	2.18	112/113	47	–	0.19
Ketone $\eta^1(O)$	39.6	1.25	1.49	2.15	–	123/117	1	133	0.13
Enol $\mu_3(C_1,C_2,O)$	52.5	1.47	1.50	2.29	2.09/2.12	108	52	–	0.18
Enol $\eta^1(C_1)$	60.8	1.33	1.42	–	2.15	122/114	7	96	0.25
Enol $\mu_2(C_1,C_2)$	79.8	1.39	1.51	–	2.09/2.19	116/110	44	–	0.21
Enolate $\eta^1(O)$	−49.5	1.33	1.36	2.02	–	127/111	0	130	0.15
Enolate $\eta^1(C_1)$	28.9	1.24	1.50	3.16	2.10	121	3	110	0.26
Enolate $\eta^1(C_1)$	37.8	1.24	1.50	3.06	2.10	121/118	2	109	0.20
Enolate $\mu_3(C_1,C_2,O)$	50.8	1.34	1.50	2.06	2.10/2.31	115/112	37	–	0.18
Enolate $\mu_2(C_1,O)$	65.2	1.25	1.48	2.12	2.06	115/126	2	–	0.10

[a] E_{ads} calculated relative to the clean surface and gas phase keto-isomer using Eq. (1).
[b] Where C_1–C_2–O differs from C_3–C_2–O the former is given first.
[c] Angle between $C_1C_2C_3$ plane and the C–O bond.
[d] The angle from C_2 through the co-ordinating atom (C_1 or O) to the metal atom for η^1(X) structures.
[e] Averaged movement of co-ordinated surface metal atoms relative to non-co-ordinated first-layer atoms.

A summary of the results for the adsorption calculations is given in Table 2. For the keto-isomer, we first consider the $\mu_2(C_2,O)$ structure shown in Fig. 2a. Here, the C–O bond is found to be considerably longer than in the reference gas phase calculation from Table 1 and is actually equal to that of the C–OH single bond in the gas phase enol-isomer. The molecule is distorted from planarity with the CC_2O angles attaining values consistent with an sp^3 hybrid geometry at C_2. The metal responds to the presence of the adsorbate by movement of the two co-ordinated Pt atoms by an average of 0.19 Å out of the surface. We also obtained a stable minima for the end-on $\eta^1(O)$ adsorption mode, shown in Fig. 2b. In this structure, the molecular plane is perpendicular to the surface but the C=O bond is tilted to place one methyl group closer to the surface than the other. The molecular geometry is only slightly perturbed from the gas phase reference calculation, with the molecular planarity preserved and deviations in bond lengths of the order of hundredths of an Ångstrom. However a strong molecule–surface interaction is present since the co-ordinated surface metal atom moves out of the surface plane by 0.13 Å and the calculated adsorption energy is 39.6 kJ mol^{-1}, some 19.1 kJ mol^{-1} more favorable than the $\mu_2(C_2,O)$ case. Indeed it appears that the $\mu_2(C_2,O)$ structure is de-stabilised by the steric repulsion between the methyl groups and the surface and that the relaxation of the surface is not able to compensate for this affect. Calculations starting with the molecular plane parallel to the surface to mimic the $\mu_2(C_2,O)$ structure, or the possibility of a $\eta^2(C_2,O)$ adsorbate, relaxed to the end-on adsorbed minimum. The $\mu_2(C_2,O)$ structure reported here was obtained by distorting the molecule so that the methyl groups are away from the surface prior to relaxation. This implies there is an energy barrier for transformation from end-on to parallel adsorption modes, which we can see from the adsorption data has a lower bound of 19.1 kJ mol^{-1}.

These results are consistent with earlier calculations, Hückel theory giving the adsorption energies of $\eta^1(O)$ and $\mu_2(C_2,O)$ as 46 and 26 kJ mol^{-1}, respectively [5] while cluster DFT models gave 45.6 and 29.7 kJ mol^{-1} [2]. We have noted previously that the neglect of extended states in the metal systems can lead to over-binding of adsorbates in cluster models [17]. The previous periodic model only reported an adsorption energy for the $\eta^1(O)$ geometry giving 19 kJ mol^{-1}. The higher binding energy reported here is likely due to the effect of surface relaxation. Experimentally TPD results have been used to derive adsorption energies for $\eta^1(O)$ acetone of 48 [4] and 49 kJ mol^{-1} [3] using the Redhead equation. The TPD peak assigned to a η^2-acetone

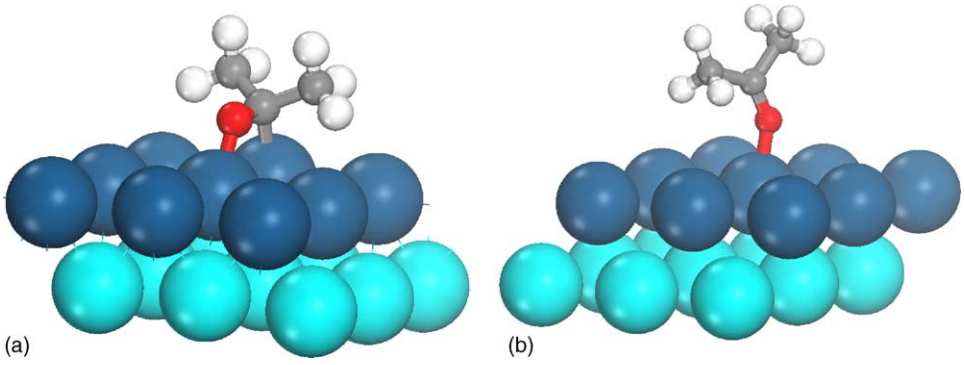

Fig. 2. Optimised structures for acetone keto-isomer adsorbed on Pt(1 1 1). (a) $\mu_2(C_2,O)$ and (b) $\eta^1(O)$ geometries. Only two-layers of the three-layer simulation slab are shown.

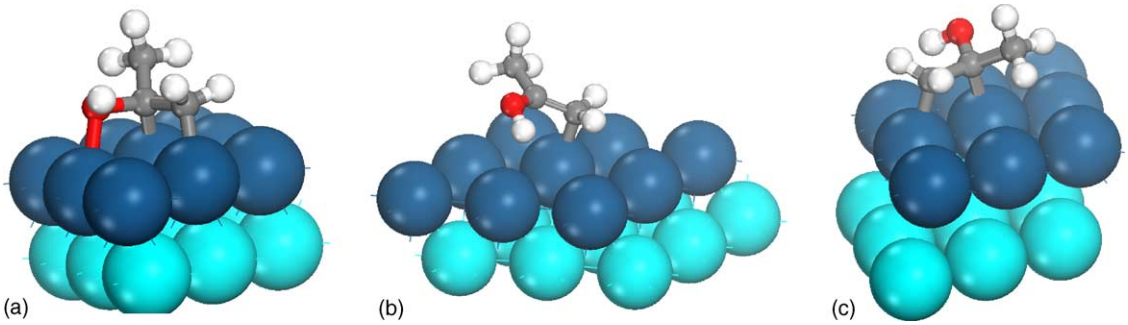

Fig. 3. Optimised structures for acetone enol-isomer adsorbed on Pt(1 1 1). (a) μ_3(C_1,C_2,O) and (b) η^1(C_1) and (c) μ_2(C_1,C_2). Only two-layers of the three-layer simulation slab are shown.

species in the work of Vannice et al. gave an adsorption energies of 52 kJ mol^{-1} [4], i.e. it was assumed that the more strongly bound species was η^2-acetone. Both our own and earlier theoretical calculations suggest that the reverse energetic ordering should occur. As mentioned in Section 1, the original experiments by Avery gave only low populations of the second species and so it was assumed that the η^2-acetone was present at step sites on the surface. In the later experiments of Vannice et al., however, care was taken to minimise the defect concentration and yet quite high surface densities of the η^2-acetone species could be prepared by flash annealing samples to 140 K. In the following, we will discuss possible alternatives for the experimental results which have been assigned to η^2-acetone species in terms of enol and enolate adsorption modes.

For the enol-isomer on Pt(1 1 1), we found no stable η^1(O) adsorption modes. However structures with a higher co-ordination number involving C atoms interacting with the surface gave stable adsorption energies relative to the gas phase ketone. The first of these is the μ_3(C_1,C_2,O) structure shown in Fig. 3a. This structure was obtained from the relaxation of a C_2,O di-σ starting point. The interaction with the surface in this μ_3(C_1,C_2,O) mode leads to a C_1–C_2 bond length comparable to that of the gas phase keto-isomer, indicating that the double bond of the enol has been significantly weakened. Similarly, the C–OH bond for this structure is elongated with respect to the gas phase enol value. The molecular planarity of the gas phase enol is also lost, with C_2 attaining an sp^3 like geometry as evidenced by the C–C_2–O angles. For a starting structure with the C=C

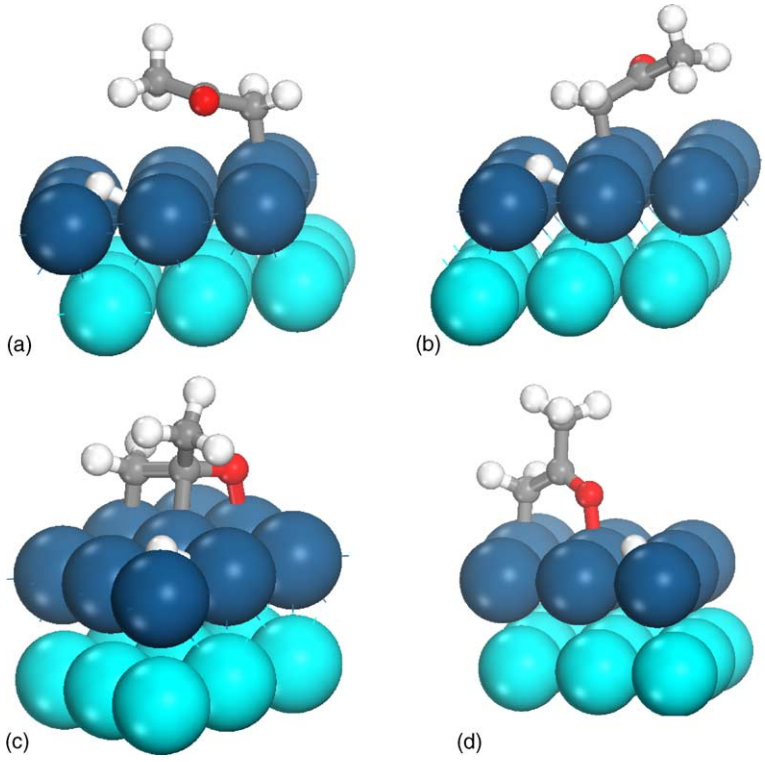

Fig. 4. Optimised structures for acetone enolate and H adsorbed on Pt(1 1 1). (a) η^1(C_1), (b) μ_2(C_1,O), (c) μ_3(C_1,C_2,O) and (d) μ_2(C_1,C_2). Only two-layers of the three-layer simulation slab are shown.

over a single Pt site the more heavily substituted carbon was found to relax away from the surface to give the $\eta^1(C_1)$ structure shown in Fig. 3b. In contrast to the $\eta^1(O)$-ketone structure, the $\eta^1(C_1)$-enol does show a lengthening of the surface co-ordinated double bond relative to the corresponding gas phase structure and the adsorption energy of $\eta^1(C_1)$-enol is also almost twice that of $\eta^1(O)$-ketone. The most favorable adsorption energy for the enol-isomer on Pt(1 1 1) was found from a C=C di-σ starting point which relaxed to the expected $\mu_2(C_1,C_2)$ geometry (Fig. 3c). Indeed the adsorption energy of this mode is 42 kJ mol^{-1} higher than that of the $\eta^1(O)$-ketone structure. In the $\mu_2(C_1,C_2)$ structure, the C=C of the enol is considerably longer than found in the gas phase and close to the value found for the C_1–C_2 single bond of the gas phase keto-isomer (Table 1), indicating that the double bond character has been reduced significantly.

The calculated enolate structures are shown in Fig. 4 and their adsorption energies and geometric parameters are also summarised in Table 2. As for the enol-isomer case, the $\eta^1(O)$-enolate structure is not found to have a favourable adsorption energy relative to the gas phase ketone. The first favourable structure is a $\eta^1(C_1)$-enolate shown in Fig. 4a. In this adsorption mode, the C_1–C_2 bond length is greater than that in the gas phase enolate and similar to the gas phase ketone, showing that the C_1–C_2 bond has a reduced bond order, as was found for the corresponding enol-isomer adsorption. A second $\eta^1(C_1)$-enolate structure was also found during these simulations (Fig. 4b). The structure of the adsorbate is practically identical to that of the structure shown in Fig. 4a, however the adsorption energy is found to be 8.9 kJ mol^{-1} more favourable. This is due to the orientation of the molecule over the surface which is different for the two $\eta^1(C_1)$-enolate structures with the more stable structure placing the methyl group over a top site whilst the other has the methyl group over a surface hollow site. This orientation means that the more stable structure also positions the oxygen atom 3.06 Å from a surface Pt atom, 0.1 Å closer than for the structure with the lower adsorption energy. The next structure observed for the enolate is a $\mu_3(C_1,C_2,O)$ mode shown in Fig. 4c. Here, the C_2–O bond is 0.1 Å longer than the previous enolate

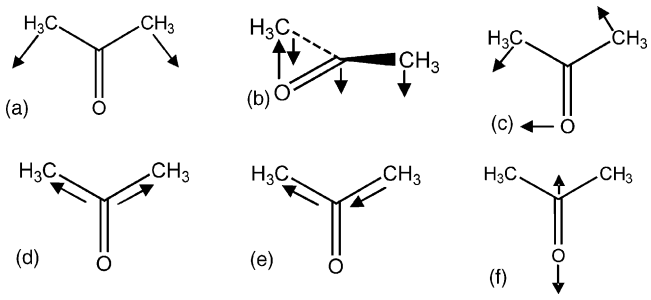

Fig. 5. The skeletal normal modes of gas phase acetone. (a) δ(MeCMe) A_1, (b) π(CO) B_2, (c) δ(CO) B_1, (d) ν_s(MeCMe) A_1, (e) ν_{as}(MeCMe) B_1 and (f) ν(CO) A_1.

structures and close to the single bond of the gas phase enol-isomer, confirming the interaction of the O atom with the surface. The C_1–C_2 bond is also longer than in the gas phase enolate calculation, attaining the same value as that in the $\eta^1(C_1)$-enolate structures. In addition, in the $\mu_3(C_1,C_2,O)$ case, the molecular planarity is lost due to the interaction of C_2 with a surface Pt atom, as can be seen from the calculated CCC–O angle.

The most stable form for the enolate-isomer that we identified has the $\mu_2(C_1,O)$ arrangement shown in Fig. 4d. In this structure, the methyl group is held perpendicular to the surface and C_1 is clearly adsorbed in an sp^3 like geometry with the hydrogen atoms rotated out of the plane of the carbon atoms. Interestingly the C–O bond has a length close to the $\eta^1(C_1)$-enolate structures in contrast to the longer C–O bond found for $\mu_3(C_1,C_2,O)$-enolate. In addition the molecule remains planar and so it is likely that the C–O bond retains some double bond character in the adsorbed state.

3.1. Vibrational analysis

In the gas phase acetone has C_{2v} symmetry, if we ignore the degrees of freedom within the methyl groups there are the six vibrations illustrated in Fig. 5, these are referred to as skeletal modes in Avery's EELS study [3]. All six skeletal modes are IR active and have been assigned from liquid phase spectra. The frequencies are given in Table 3 along with calculated data from this study and surface science

Table 3
Vibrational frequencies for adsorbates on Pt(1 1 1) from DFT calculations and reference data

	Ketone gas phase, DFT (symmetry)[a]	$\eta^1(O)$-ketone, DFT	Ketone DFT $\mu_2(C_2,O)$	Enolate DFT $\mu_2(C_1,O)$	IR liquid[b]	$\eta^1(O)$, HREELS[c]	Species 2, RAIRS/HREELS[c]
ν(CO)	1737 (A_1)	1600	1161	1574	1710	1640	1610/1530–1585/1511
ν_a(MeCMe)	1200 (B_1)	1227	1330	1228	1220	1250	1240
ν_s(MeCMe)	775 (A_1)	805	775	835	783	810	830
δ(CO)	509 (B_1)	546	445	580	530	550	
π(CO)	461 (B_2)	470	588	602	484		
δ(MeCMe)	372 (A_1)	387	416	383	390		350

Notes: All frequencies reported in cm^{-1}.

[a] Symmetry based on gas phase acetone in C_{2v} symmetry, as illustrated in Fig. 5.

[b] Data from reference [3].

[c] Data from reference [4], species 2 refers to the spectra assigned to η^2-acetone in the reference.

measurements for adsorbed species from HREELS and RAIRS [4]. The highest frequency mode is for the C=O stretch which occurs at 1710 cm^{-1} in the liquid state. Periodic DFT calculations give a small over estimate placing the C=O stretch for an isolated acetone model at 1737 cm^{-1}. The more complex bending modes tend to be under estimated by a similar amount. These differences from experiment of around 2% are consistent with other DFT based vibrational mode calculations [18].

As pointed out by Avery the molecular symmetry can be lowered on adsorption either by tilting to make the methyl groups in-equivalent, in which case the mirror plane perpendicular to the molecular plane is lost, or by tilting while maintaining the equivalence of the methyl groups, in which case the plane of the molecule is no longer a symmetry element. A combination of these two effects could also lead to a C_1 structure. By considering the observed vibrations it was found that, on Pt(1 1 1), the η^1(O)-ketone adsorbate is tilted to give C_s symmetry but the two alternative tilting modes could not be distinguished. Our calculations are consistent with the first C_s structure, tilted to give in-equivalent methyl groups. Optimisations to locate the alternative C_s arrangement lead only to minima with binding energies around 30 kJ mol^{-1} less favorable than that reported here.

The calculated vibrational frequencies for this η^1(O)-ketone shows a reduction in the C=O stretch frequency compared to the gas phase reference state of 137 cm^{-1} which should be compared with the experimental shift of 70 cm^{-1}. By inspection of animations of the vibrational modes we were able to confirm the symmetry assignments of each skeletal vibrational mode. In agreement with the EELS data both methyl stretch vibrations and δ(CO) (wagging of CO in the plane of the molecule) increase in frequency on adsorption to the surface, experimentally the shifts are 30, 27 and 20 cm^{-1}, respectively, compared to the DFT calculated shifts of 27, 30 and 37 cm^{-1}. Given the errors in the absolute vibrational frequencies calculated and the low intensity of the experimental δ(CO) band this agreement is reasonable.

We have also sought candidates for the second species for which vibrational spectra has been reported by Vannice et al. [4]. For the only parallel adsorbed ketone structure, μ_2(C_2,O), we see a C–O stretch frequency which is greatly reduced compared to the gas phase ketone with a shift of 576 cm^{-1}. Although several bands are reported in the reference data of Table 3 the maximum experimental shift is much less dramatic, at most 200 cm^{-1}. As discussed earlier this di-σ bonded μ_2(C_2,O) structure appears to be strongly distorted by the interaction with the surface and the elongation of the C–O bond observed is consistent with this low calculated vibrational frequency. This means that the experimental assignment to a η^2(C_2,O) adsorbate is probably incorrect and so we compare the experimental vibrational bands with calculations on the alternative species discussed above. The enol structures all have a formally single C–O bond and show similar low frequencies for the C–O stretch to that found for μ_2(C_2,O)-ketone. The vibrational frequencies calculated for the enolate structure with the most favourable adsorption energy, μ_2(C_1,O), are reported in Table 3 and show much closer agreement with the experimental data of species 2. The CO stretch is in the range of values quoted experimentally and the methyl stretching frequencies show similar shifts from the reference free acetone data. The relatively small shift of the CO stretch is also consistent with the observation that the calculated CO bond length is almost the same as that of the free enolate reference structure.

4. Conclusions

We have considered the adsorption of acetone to Pt(1 1 1) in various orientations and in three possible isomeric forms. In the gas phase, the ketone is considerably more stable than the enol or enolate and so any adsorption process will begin with the ketone interacting with the surface. The keto-isomer is found to be around 19 kJ mol^{-1} more strongly adsorbed in an end-on, η^1(O), configuration than the alternative μ_2(C_2,O) adsorption parallel to the surface. This energy difference is caused by the steric interaction between the methyl groups and the surface and so is likely to be common to any substituted ketone adsorbed parallel to the surface. The agreement between the calculated vibrational modes of the η^1(O)-ketone and experimental EELS data is good for all the skeletal modes of the molecule. The μ_2(C_2,O)-ketone has a considerably longer C–O bond than in the gas phase ketone with a correspondingly lowered C–O stretch frequency. This makes it unlikely that the second species identified in the surface spectroscopy experiments is a ketone adsorbed parallel to the surface. In addition experimental TPD data suggests that this second species is more strongly bound than the η^1(O)-ketone which is not supported by our own or earlier calculations.

We conclude that the most likely explanation for the second species observed in the surface science experiments for acetone on Pt(1 1 1) is a μ_2(C_1,O) enolate. This would mean that deprotonation of acetone can take place on the clean Pt surface even at the low temperatures of the surface science experiments. This may not be unreasonable since similar species have recently been observed on the (1 1 1) surface of Ni [8].

The main implication for the dimer model used to predict selectivity in enantioselective hydrogenation is that the inferred tendency of the ketone groups to favour a pyruvate ester molecule adsorbed parallel to the surface is incorrect. It is more likely that the role of the modifier is to interact with an end-on adsorbed ketone group and for this interaction to tilt the plane of the molecule toward the surface, thereby allowing hydrogenation to take place.

The results presented here also suggest that there will be enol and enolate species present on the Pt surface during hydrogenation of ketones for which keto–enol isomerisation is possible. In the case of pyruvate ester hydrogenation on Pt

the kinetic studies of Wells discussed in the Introduction suggest that these species are spectators or lead to side products. However, over Pd deuteration of the methyl group is observed and so there must be hydrogenation through the enol or enolate species. Competitive hydrogenation of ketone and enol/enolate may explain the lower *e.e*. observed for Pd. The calculations to date have been based only on the relative adsorption energies of the alternative isomers. We are currently working to locate the transition states for their inter-conversion so that the kinetic interchange of species can be discussed.

Acknowledgements

This project was funded, in part, from an EPSRC IMI project involving Johnson Matthey, BP-Amoco, Robinson Brothers, Grace Davidson and Accelrys. Time on the UK HPCx facility was obtained through the Materials Consortium.

References

[1] O. Schwalm, J. Weber, B. Minder, A. Baiker, Int. J. Quant. Chem. 52 (1994) 191;
K.E. Simons, P.A. Meheux, S.P. Griffiths, I.M. Sutherland, P. Johnston, P.B. Wells, A.F. Carley, M.K. Rajumon, M.W. Roberts, A. Ibbotson, Recl. Trac. Chim. Pays-Bas 113 (1994) 465.
[2] A. Vargas, T. Burgi, A. Baiker, J. Catal. 222 (2004) 439.
[3] N.R. Avery, Surf. Sci. 125 (1983) 771.
[4] M.A. Vannice, W. Erley, H. Ibach, Surf. Sci. 254 (1991) 1.
[5] F. Delbecq, P. Sautet, Surf. Sci. 295 (1993) 353.
[6] R. Alcalá, J. Greeley, M. Mavrikakis, J.A. Dumesic, J. Chem. Phys. 116 (2002) 8973.
[7] T.J. Hall, P. Johnston, W.A.H. Vermeer, S.R. Watson, P.B. Wells, Stud. Surf. Sci. Catal. 101 (1996) 221.
[8] W.-S. Sim, T.C. Li, P.-X. Yang, B.-S. Yeo, J. Am. Chem. Soc. 124 (2002) 4970.
[9] G. Kresse, J. Furthmüller, Phys. Rev. B 54 (1996) 11169;
G. Kresse, J. Furthmüller, Comput. Mater. Sci. 6 (1996) 15.
[10] J.P. Perdew, J.A. Chevary, S.H. Vorto, K.A. Jackson, M.R. Pedersen, D.J. Singh, C. Frolhais, Phys. Rev. B 46 (1992) 6671.
[11] P.E. Blöchl, Phys. Rev. B 50 (1994) 17953;
G. Kresse, D. Joubert, Phys. Rev. B 59 (1999) 1758.
[12] G. Kresse, J. Hafner, J. Phys. Condens. Matter 6 (1994) 8245.
[13] G.C. Bond, J. Mol. Catal. A 156 (2000) 1.
[14] H.J. Monkhurst, J.D. Pack, Phys. Rev. B 13 (1976) 5188.
[15] G.W. Watson, R.P.K. Wells, D.J. Willock, G.J. Hutchings, J. Phys. Chem. B 105 (2001) 4889.
[16] G.A. Somorjai, Surface Chemistry and Catalysis, John Wiley & Sons, New York, 1994, ISBN 0471031925.
[17] G.W. Watson, R.P.K. Wells, D.J. Willock, G.J. Hutchings, Surf. Sci. 459 (2000) 93.
[18] D. Loffreda, Y. Jugnet, F. Delbecq, J.C. Bertolini, P. Sautet, J. Phys. Chem. B 108 (2004) 9085.